Phonon Frequencies of the Hexagonal Metals Be, Mg, and Zn

SATYA PRAKASH AND S. K. JOSHI
Physics Department, University of Roorkee, Roorkee, India
(Received 16 June 1969)

The phonon frequencies of hexagonal metals Be, Mg, and Zn are computed using the single-orthogonalized-plane-wave electron-ion matrix element and the dielectric function due to Singwi *et al.* The bare-ion potential is obtained by a modified Hartree-Fock-Slater scheme. The exchange potential is determined by the Kohn-Sham approach, and the correlation corrections are included according to the prescription of Robinson *et al.* The calculated phonon frequencies of these metals are in good agreement with the neutron spectrometric measurements, except for Zn in the $[01\bar{1}0]$ direction. The phonon frequencies for these metals are also calculated for different c/a ratios.

I. INTRODUCTION

IN recent years, a number of detailed neutron spectrometric measurements of the phonon frequencies along the symmetry directions have been completed for the hexagonal close-packed (hcp) metals Be,[1] Mg,[2] and Zn.[3] The axial ratio c/a is 1.6333 for ideal close packing for this structure. Actually, this ratio for hcp metals is found to be different from the ideal value. For Be it is as low as 1.5677 and for Zn it has a high value of 1.8565. The axial ratio is very close to the ideal value for Mg resulting in a large measure of isotropy in the elastic properties of Mg. The experimental data for phonon frequencies have been analyzed on the basis of the force-constant models[4] for these metals. Roy *et al.* used the pseudopotential approach[5] to calculate the phonon frequencies of Mg. They found that the use of a pseudopotential, calculated from the first principles,[6] led to imaginary phonon frequencies in the longitudinal acoustic (LA) branch for the phonon wave vector $q<0.5q_{\max}$ in the [0001] direction. Finally, they employed the two-parameter model potential proposed by Harrison,[7] and their calculations agreed with the measurements of Iyengar *et al.*[2] Brovman, Kagan, and Holas,[8] and Schneider and Stoll[9] also used the model-pseudopotential approach to calculate the phonon frequencies of these metals. Koppel and Yong[10] followed the pseudopotential method due to Sham to calculate the phonon frequencies of Be. Gilat, Rizzi, and Cubiotti[11] used the optimum-model pseudopotential to calculate the phonon frequencies of Be, Mg, and Zn. The agreement of their calculations with experiment is quite good.

Recently, we[12] calculated the phonon frequencies of alkali metals using the single-orthogonalized-plane-wave (OPW) theory of electron-ion matrix element (EIME) put forth by Vosko *et al.*[13] and the dielectric function due to Singwi *et al.*[14] It is worthwhile to extend the single-OPW theory of EIME to calculate the phonon frequencies of hcp metals. The studies of the band structure and Fermi surfaces of these metals reveal that a nearly-free-electron model is a good approximation for them.[15–18] The use of the single-OPW EIME, is, therefore, not unjustified for these metals.

We present in Sec. II an abbreviated resume of the formulation of the single-OPW EIME to introduce the notation. The method of calculating the crystal potential and a comparison with the potential used in the band-structure calculations are also presented there. The results for the phonon frequencies of Be, Mg, and Zn are discussed in Sec. III.

II. THEORY

The hcp structure consists of two interpenetrating simple hexagonal lattices. If c is the distance between two alternate planes and a is the distance between nearest neighbors in any plane, the lattice may be described as a Bravais lattice with a basis, the unit cell having the edges

$$\mathbf{a}_1=a\hat{\imath}\,,\quad \mathbf{a}_2=-\tfrac{1}{2}a\hat{\imath}+\tfrac{1}{2}a\sqrt{3}\hat{\jmath}\quad\text{and}\quad \mathbf{a}_3=c\hat{k}\,,$$

[1] R. E. Schmunk, Phys. Rev. **149**, 450 (1966).
[2] P. K. Iyengar, G. Venkataraman, P. R. Vijayaraghavan, and A. P. Roy, in *Inelastic Scattering of Neutrons* (International Atomic Energy Agency, Vienna, 1965), Vol. I, p. 153.
[3] D. L. McDonald, M. M. Elcombe, and A. W. Pryor (private communication).
[4] E. A. Metzbower, Phys. Rev. **177**, 1139 (1969). Other references to the force-constant models for hcp metals are given in this paper.
[5] A. P. Roy and G. Venkataraman, Phys. Rev. **156**, 769 (1967). There are a few errors in this paper which are corrected by Roy and Venkataraman (private communication).
[6] W. A. Harrison, *Pseudopotentials in the Theory of Metals* (W. A. Benjamin, Inc., New York, 1966).
[7] W. A. Harrison, Phys. Rev. **139**, A176 (1965).
[8] E. G. Brovman, Yu. Kagan, and A. Holas, in *Neutron Inelastic Scattering* (International Atomic Energy Agency, Vienna, 1968), Vol. I, p. 165.
[9] T. Schneider and E. Stoll, in *Neutron Inelastic Scattering* (International Atomic Energy Agency, Vienna, 1968), Vol. I, p. 101.
[10] J. U. Koppel and J. A. Yong, in *Neutron Thermalization and Reactor Spectra* (International Atomic Energy Agency, Vienna, 1968), Vol. I, p. 333.
[11] G. Gilat, G. Rizzi, and G. Cubiotti, Phys. Rev. (to be published).
[12] S. Prakash and S. K. Joshi, Phys. Rev. (to be published).
[13] S. H. Vosko, R. Taylor, and G. H. Keech, Can. J. Phys. **43**, 1187 (1965).
[14] K. S. Singwi, M. P. Tosi, R. H. Land, and A. Sjölander, Phys. Rev. **176**, 589 (1968).
[15] J. H. Tripp, W. L. Gordon, P. M. Everett, and R. W. Stark, Phys. Letters **26A**, 98 (1967).
[16] R. W. Stark, Phys. Rev. **162**, 589 (1967).
[17] W. J. O'Sullivan and J. E. Shirber, Phys. Rev. **162**, 519 (1967).
[18] J. C. Kimball, R. W. Stark, and F. M. Mueller, Phys. Rev. **162**, 66 (1967),

as shown in Fig. 1. The unit cell contains two atoms, one at the origin **O** and the other at $\frac{1}{3}\mathbf{a}_1+\frac{2}{3}\mathbf{a}_2+\frac{1}{2}\mathbf{a}_3$. The convention employed in this calculation, for the orientations of the hexagonal lattice vectors $\mathbf{a}_1$, $\mathbf{a}_2$, $\mathbf{a}_3$, and for the reciprocal-lattice vectors $\mathbf{b}_1$, $\mathbf{b}_2$, $\mathbf{b}_3$ with respect to Cartesian axes is shown in Fig. 1. The volume of the unit cell is $\Omega_0=\frac{1}{2}a^2c\sqrt{3}$ and atomic radius r_s is defined by $\frac{4}{3}\pi r_s^3=\frac{1}{2}\Omega_0$. The radius of the free-electron Fermi sphere k_F and the volume of the Brillouin zone Ω_k are related to Ω_0 by

$$\tfrac{1}{2}\times\tfrac{4}{3}\pi k_F^3=\Omega_k=\frac{8\pi^3}{\Omega_0}.$$

A. Dynamical Matrix and Electron-Phonon Interaction

The general expression for the phonon frequencies corresponding to the phonon wave vector $\mathbf{q}$ is given by[19]

$$\omega^2 a_x(j)=\sum_{j',y} D_{xy}(\mathbf{q},jj')a_y(j'), \tag{1}$$

where $a_x(j)$ is the x component of the amplitude vector $\mathbf{a}(j)$ for the jth atom in the unit cell. $D_{xy}(\mathbf{q},jj')$ is the usual dynamical matrix

$$D_{xy}(\mathbf{q},jj')=\frac{1}{M}\sum_{l'}\Phi_{xy}(l',jj')\times\exp\{-i\mathbf{q}\cdot[\mathbf{r}(j)-\mathbf{r}(l')-\mathbf{r}(j')]\},\quad \text{for}\quad j'\neq j \tag{2}$$

and

$$D_{xy}(\mathbf{q},jj)=\frac{1}{M}\Big(\sum_{l'}\Phi_{xy}(l',jj)\exp[i\mathbf{q}\cdot\mathbf{r}(l')]-\sum_{l'}\Phi_{xy}(l',jj)-\sum_{j'\neq j}\sum_{l'}\Phi_{xy}(l',jj')\Big). \tag{3}$$

We have chosen a point in the lth cell as the origin. $\mathbf{r}(l')$ is the position vector of the corresponding point in the l'th unit cell, and from this point the j'th atom in the same cell is at a distance $\mathbf{r}(j')$. The quantity $\Phi_{xy}(l',jj')$ is the usual force constant, and M is the mass of the ion. In further discussion we drop the prime over l. $\Phi_{xy}(l,jj')$ and, hence, the dynamical matrix $D_{xy}(\mathbf{q},jj')$ is written as the sum of the three contributions.[20]

$$D_{xy}(\mathbf{q},jj')=D_{xy}^{(C)}(\mathbf{q},jj')+D_{xy}^{(E)}(\mathbf{q},jj')+D_{xy}^{(R)}(\mathbf{q},jj'). \tag{4}$$

$D_{xy}^{(C)}$ arises from the bare Coulomb interaction between ions, $D_{xy}^{(R)}$ is due to exchange-overlap potential between ion cores, and $D_{xy}^{(E)}$ originates from the ion-electron-ion interaction, which also includes electron-electron interaction.

The $D_{xy}^{(C)}$ is evaluated with the help of Ewald's θ-function transformation,[21,22] and the explicit expression for $D_{xy}^{(C)}$ is

$$\begin{aligned}D_{xy}^{(C)}(\mathbf{q},jj')=&\frac{4\pi(Z^*e)^2}{M\Omega_0}\sum_{\mathbf{H}}\frac{(\mathbf{q}+\mathbf{H})_x(\mathbf{q}+\mathbf{H})_y}{|\mathbf{q}+\mathbf{H}|^2}\exp(-|\mathbf{q}+\mathbf{H}|^2/4\eta^2)\exp(i\mathbf{H}\cdot\mathbf{r}_{jj'})\\&-\frac{(Z^*e)^2}{M}\sum_{l}\Bigg\{\frac{[\mathbf{r}(l,jj')]_x[\mathbf{r}(l,jj')]_y}{|\mathbf{r}(l,jj')|^5}\Bigg[3\,\mathrm{erf}(\eta|\mathbf{r}(l,jj')|)+\Bigg(\frac{4\eta^3|\mathbf{r}(l,jj')|^3}{\sqrt{\pi}}+\frac{6\eta|\mathbf{r}(l,jj')|}{\sqrt{\pi}}\Bigg)\exp(-\eta^2|\mathbf{r}(l,jj')|^2)\Bigg]\\&-\frac{\delta_{xy}}{|\mathbf{r}(l,jj')|^3}\Bigg[\mathrm{erf}(\eta|\mathbf{r}(l,jj')|)+\frac{2\eta|\mathbf{r}(l,jj')|}{\sqrt{\pi}}\exp(-\eta^2|\mathbf{r}(l,jj')|^2)\Bigg]\Bigg\}\exp[-i\mathbf{q}\cdot\mathbf{r}(l,jj')],\quad \text{for}\quad j\neq j'\end{aligned} \tag{5}$$

and

$$\begin{aligned}D_{xy}^{(C)}(\mathbf{q},jj')=&\frac{4\pi(Z^*e)^2}{M\Omega_0}\Bigg[\sum_{\mathbf{H}}\frac{(\mathbf{q}+\mathbf{H})_x(\mathbf{q}+\mathbf{H})_y}{|\mathbf{q}+\mathbf{H}|^2}\exp\Bigg(-\frac{|\mathbf{q}+\mathbf{H}|^2}{4\eta^2}\Bigg)-\sum_{\mathbf{H}\neq 0}\frac{H_xH_y}{H^2}\exp\Bigg(-\frac{H^2}{4\eta^2}\Bigg)\Bigg]\\&-\frac{(Z^*e)^2}{M}\sum_{l\neq 0}[\exp(i\mathbf{q}\cdot\mathbf{r}(l))-1]\Bigg\{\frac{[\mathbf{r}(l)]_x[\mathbf{r}(l)]_y}{|\mathbf{r}(l)|^5}\Bigg[3\,\mathrm{erf}[\eta|\mathbf{r}(l)|]+\Bigg(\frac{4\eta^3|\mathbf{r}(l)|^3}{\sqrt{\pi}}+\frac{6\eta|\mathbf{r}(l)|}{\sqrt{\pi}}\Bigg)\\&\times\exp[-\eta^2|\mathbf{r}(l)|^2]\Bigg]-\frac{\delta_{xy}}{|\mathbf{r}(l)|^3}\Bigg[\mathrm{erf}[\eta|\mathbf{r}(l)|]+\frac{2\eta|\mathbf{r}(l)|}{\sqrt{\pi}}\exp[-\eta^2|\mathbf{r}(l)|^2]\Bigg]\Bigg\}\\&-\sum_{j\neq j'}\Bigg[\frac{4\pi(Z^*e)^2}{M\Omega_0}\sum_{\mathbf{H}\neq 0}\frac{H_xH_y}{|\mathbf{H}|^2}\exp\Bigg(-\frac{|\mathbf{H}|^2}{4\eta^2}\Bigg)\exp(i\mathbf{H}\cdot\mathbf{r}_{jj'})-\frac{(Z^*e)^2}{M}\sum_{l}\Bigg\{\frac{[\mathbf{r}(l,jj')]_x[\mathbf{r}(l,jj')]_y}{|\mathbf{r}(l,jj')|^5}\Bigg[3\,\mathrm{erf}[\eta|\mathbf{r}(l,jj')|]\\&+\Bigg(\frac{4\eta^3|\mathbf{r}(l,jj')|^3}{\sqrt{\pi}}+\frac{6\eta|\mathbf{r}(l,jj')|}{\sqrt{\pi}}\Bigg)\exp[-\eta^2|\mathbf{r}(l,jj')|^2]\Bigg]-\frac{\delta_{xy}}{|\mathbf{r}(l,jj')|^3}\Bigg[\mathrm{erf}[\eta|\mathbf{r}(l,jj')|]+\frac{2\eta|\mathbf{r}(l,jj')|}{\sqrt{\pi}}\\&\times\exp[-\eta^2|\mathbf{r}(l,jj')|^2]\Bigg]\Bigg\}\Bigg].\end{aligned} \tag{6}$$

[19] S. K. Joshi and A. K. Rajagopal, in *Solid State Physics*, edited by F. Seitz and D. Turnbull (Academic Press Inc., New York, 1968), Vol. 22, p. 159; M. Born and K. Huang, *Dynamical Theory of Crystal Lattices* (Oxford University Press, London, 1954), p. 224.
[20] T. Toya, J. Res. Inst. Catalysis, Hokkaido Univ. 6, 183 (1958).
[21] P. P. Ewald, Ann. Phys. (4) 64, 253 (1921).
[22] E. W. Kellerman, Phil. Trans. Roy. Soc. London A238, 513 (1940).

Here

$$\mathrm{erf}(x)=1-\frac{2}{\sqrt{\pi}}\int_0^x e^{-x^2}dx \tag{7}$$

and

$$\mathbf{r}(l,jj')=\mathbf{r}_j-\mathbf{r}_{j'}-\mathbf{r}(l)$$
$$=\mathbf{r}_{jj'}-\mathbf{r}(l).$$

Z^* is the effective charge of the ion, $\mathbf{H}$ is the reciprocal-lattice vector, and e is the electronic charge. The parameter η is chosen to render the series in the direct and in the reciprocal space in Eqs. (5) and (6), quickly convergent.

The ionic radii of the metals under consideration are small as compared to the lattice spacings. The calculated core wave functions were also found to be compact. Only a negligible tail of a core wave function exists beyond $\mathbf{r}_s$. Therefore, we have ignored the contribution $D_{xy}{}^{(R)}$ which arises from the exchange-overlap potential between ion cores.

The electronic contribution $D_{xy}{}^{(E)}$ is expressed as

$$D_{xy}{}^{(E)}(\mathbf{q},jj')=-(1/M\Omega_0)\sum_{\mathbf{H}}E_{xy}(|\mathbf{q}+\mathbf{H}|)$$
$$\times\exp(i\mathbf{H}\cdot\mathbf{r}_{jj'}),\quad \text{for}\quad j\neq j' \tag{8}$$

and

$$D_{xy}{}^{(E)}(\mathbf{q},jj)=-(1/M\Omega_0)\Big[\sum_{\mathbf{H}}E_{xy}(|\mathbf{q}+\mathbf{H}|)$$
$$-\sum_{\mathbf{H}\neq 0}E_{xy}(H)-\sum_{j\neq j'}\sum_{\mathbf{H}\neq 0}E_{xy}(H)\exp(i\mathbf{H}\cdot\mathbf{r}_{jj'})\Big]. \tag{9}$$

In the single-OPW theory of EIME due to Vosko *et al.*,[13] the explicit expression for $E_{xy}(p)$ is

$$E_{xy}(p)=E_{xy}{}^{(1)}(p)+E_{xy}{}^{(2)}(p), \tag{10}$$

with

$$E_{xy}{}^{(1)}(p)=-4\pi Z^{*2}e^2(p_xp_y/p^2)[S(p)/(p^2+S(p))]$$
$$\times[\mathcal{G}(pr_s)-\zeta p^2U_0(p)]^2 \tag{11}$$

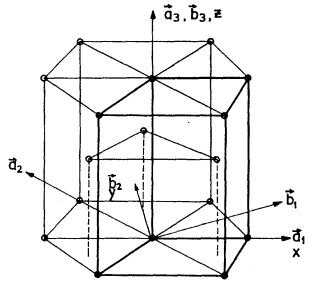

FIG. 1. Direct lattice vectors $\mathbf{a}_1$, $\mathbf{a}_2$, and $\mathbf{a}_3$; reciprocal-lattice vectors $\mathbf{b}_1$, $\mathbf{b}_2$, and $\mathbf{b}_3$; and Cartesian axes x, y, and z for hcp structure.

and

$$E_{xy}{}^{(2)}(p)=-4\pi Z^{*2}e^2\frac{p_xp_y}{p^2}\{-[p^2/(p^2+S(p))][2(\mathcal{G}(pr_s)$$
$$-\zeta p^2U_0(p))+\zeta(B_1g_1+C_1g_2)+2D_1]$$
$$\times[\zeta(B_1g_1+C_1g_2)+2D_1]+\zeta^2p^2(B_1{}^2g_2$$
$$+2B_1C_1g_3+C_1{}^2g_4)+2\zeta p^2(2D_2+p^2a_0{}^2+D_3)\}. \tag{12}$$

Here,

$$\zeta=0.5\Omega_0/8\pi Z^*a_0, \tag{13}$$

$$U_0(p)=U_s(p)+A_1(p), \tag{14}$$

and $\mathbf{p}$ is a general vector in the reciprocal space. $\mathcal{G}(pr_s)$ is the Fourier transform of the unit step function in the atomic sphere. $U_s(p)$ is the Fourier transform of the crystal potential which enters the solution of the Schrödinger equation for core eigenvalues and core eigenfunctions. A_i, B_i, and C_i are the expansion coefficients for the $\mathbf{k}$-dependent (electron wave vector) part of the EIME. The D_i are functions of k_F/p, A_i, B_i, and C_i, while the g_i are functions of k_F/p alone. The explicit expressions for these quantities are given in the paper of Vosko *et al.*[13] a_0 is the Bohr radius and $S(p)$ is the proper polarization function for the conduction electrons. On the basis of our earlier experience with alkali metals, we have used the polarization function due to Singwi *et al.*[14] which is essentially a modified version of the Hubbard polarization function.[23] The polarization function due to Singwi *et al.* is given by

$$S_s(p)=S_0(p)/[1-Q(p)S_0(p)], \tag{15}$$

where $S_0(p)$ is the polarization function for free electrons,

$$S_0(p)=\frac{2k_F}{\pi a_0}\left(1+\frac{4k_F{}^2-p^2}{4k_Fp}\ln\left|\frac{p+2k_F}{p-2k_F}\right|\right), \tag{16}$$

and

$$Q(p)=\frac{9}{32k_F{}^2}\Big\{\frac{2}{105}\Big[24\Big(\frac{k_F{}^2}{p^2}\Big)+44+\Big(\frac{p}{k_F}\Big)^2\Big]$$
$$-\frac{2k_F}{p}\Big[\frac{8}{35}\Big(\frac{k_F}{p}\Big)^2-\frac{4}{15}+\frac{1}{6}\Big(\frac{p}{k_F}\Big)^2\Big]\ln\left|\frac{p+2k_F}{p-2k_F}\right|$$
$$+\Big(\frac{p}{k_F}\Big)^2\Big[\frac{1}{210}\Big(\frac{p}{k_F}\Big)^2-\frac{2}{15}\Big]\ln\left|\frac{p^2-4k_F{}^2}{p^2}\right|\Big\}. \tag{17}$$

In the calculation of $D_{xy}{}^{(E)}(\mathbf{q},jj')$ and $D_{xy}{}^{(E)}(\mathbf{q},jj)$, we choose the jth atom as the origin, i.e., $\mathbf{r}_j=(0,0,0)$ and $\mathbf{r}_{j'}=\frac{1}{3}\mathbf{a}_1+\frac{2}{3}\mathbf{a}_2+\frac{1}{2}\mathbf{a}_3$. Then, Eqs. (8) and (9) can be

[23] J. Hubbard, Proc. Roy. Soc. (London) **A243**, 336 (1957).

written as

$$D_{xy}{}^{(E)}(\mathbf{q},jj')=-\frac{1}{M\Omega_0}\sum_{\mathbf{H}}E_{xy}(|\mathbf{q}+\mathbf{H}|)\times[\cos(\mathbf{H}\cdot\mathbf{r}_{j'})-i\sin(\mathbf{H}\cdot\mathbf{r}_{j'})] \quad (18)$$

and

$$D_{xy}{}^{(E)}(\mathbf{q},jj)=-\frac{1}{M\Omega_0}\{\sum_{\mathbf{H}}E_{xy}(|\mathbf{q}+\mathbf{H}|)-\sum_{\mathbf{H}\neq 0}E_{xy}(H)[1-\cos(\mathbf{H}\cdot\mathbf{r}_j')]\}. \quad (19)$$

The contribution to the sum over $\mathbf{H}$ from the imaginary part in the last term in Eq. (9) vanishes. $D_{xy}(\mathbf{q},jj')$ and $D_{xy}(\mathbf{q},jj)$ are evaluated with the help of Eqs. (4)–(6), (18), and (19). The phonon frequencies are calculated along the principal symmetry directions using the expressions given below, obtained by Czachor[24] by factorizing the secular equation.

(a) [0001] direction, z polarization, longitudinal mode:

$$\omega^2(q_z)=D_{zz}(\mathbf{q},jj)\pm|D_{zz}(\mathbf{q},jj')|, \quad (q_x=q_y=0;\ q_z=q_z). \quad (20a)$$

(b) [0001] direction, x or y polarization, transverse modes:

$$\omega^2(q_z)=D_{xx}(\mathbf{q},jj)\pm|D_{xx}(\mathbf{q},jj')|, \quad (q_x=q_y=0;\ q_z=q_z). \quad (20b)$$

(c) [01$\bar{1}$0] direction, y polarization, longitudinal mode:

$$\omega^2(q_y)=D_{yy}(\mathbf{q},jj)\pm|D_{yy}(\mathbf{q},jj')|, \quad (q_x=q_z=0;\ q_y=q_y). \quad (21a)$$

(d) [01$\bar{1}$0] direction, x polarization, transverse mode $\parallel$ to basal plane:

$$\omega^2(q_y)=D_{xx}(\mathbf{q},jj)\pm|D_{xx}(\mathbf{q},jj')|, \quad (q_x=q_z=0;\ q_y=q_y). \quad (21b)$$

(e) [01$\bar{1}$0] direction, z polarization, transverse mode $\perp$ to basal plane:

$$\omega^2(q_y)=D_{zz}(\mathbf{q},jj)\pm|D_{zz}(\mathbf{q},jj')|, \quad (q_x=q_z=0;\ q_y=q_y). \quad (21c)$$

The plus sign is for the optical mode while the minus sign is for the acoustic mode.

B. Crystal Potential

We observe in Eqs. (11) and (12) that the Fourier transform of the crystal potential enters the expression for the electronic part of the dynamical matrix. The crystal potential also occurs in the Schrödinger equation, which yields the core eigenvalues and core eigenfunctions which are used in the evaluation of expansion coefficients A_i, B_i, and C_i. It is, therefore, desirable that we should use a reliable but not too intricate potential in our calculations. To a fair approximation, the crystal potential $U_s(r)$ may be taken as the sum of the bare-ion potential $U_b(r)$ and the conduction-electron potential $U_e(r)$:

$$U_s(r)=U_b(r)+U_e(r). \quad (22)$$

$U_b(r)$ is evaluated by a modified Hartree-Fock-Slater (HSF) scheme[25] which includes (a) the potential due to the ion core and (b) the exchange and correlation contributions of core electrons. The mutual exchange between core and conduction electrons is neglected. The Slater-exchange potential[26] is replaced by the Kohn-Sham-exchange potential,[27] and correlation corrections are added according to the simple prescriptions of Robinson *et al.*[28] This leads to a screened-exchange potential

$$V_{\text{sc ex}}(r)=-4[(3/8\pi)\rho(r)R^3(\alpha)]^{1/3}, \quad (23)$$

where

$$R(\alpha)=1-\tfrac{4}{3}\alpha\tan^{-1}(2/\alpha)+\tfrac{1}{2}\alpha^2\ln|1+4/\alpha^2|-\tfrac{1}{6}\alpha^2[1-\tfrac{1}{4}\alpha^2\ln(1+4/\alpha^2)], \quad (24)$$

and $\alpha=(k_s/k_F)=0.646[\rho(r)]^{-1/6}$. Here, k_s is the Thomas-Fermi screening length. The electron density $\rho(r)$ is

$$\rho(r)=(1/4\pi)\sum_{n,l(\text{core})}2(2l+1)(p_{nl}{}^2(r)/r^2). \quad (25)$$

Here, n and l are the usual quantum numbers $p_{nl}(r)=rR_{nl}(r)$, and $R_{nl}(r)$ is the radial part of the core wave function. The potential $U_e(r)$, due to the conduction electrons and assumed to be uniformly distributed in the Wigner-Seitz cell, is written as the sum of Coulomb and screened-exchange potentials, i.e.,

$$U_e(r)=2(3/r_s-r^2/r_s{}^3)-(1.5392/r_s)R(\alpha), \quad \text{for } r\leq r_s \quad (26a)$$

$$=4/r-(1.5392/r_s)R(\alpha), \quad \text{for } r>r_s. \quad (26b)$$

Here, $R(\alpha)$ is evaluated for the uniform density of the conduction electrons. Again, we have ignored the potential due to deviation from spherical symmetry of the Wigner-Seitz cell. The crystal potential calculated by us does not show the humps which are present in more accurate potentials of Loucks and Cutler[29] and of Falicov[30] for Be and Mg, respectively. These humps arise from the consideration of exchange between the core and the conduction electrons. When we use the

[24] A. Czachor, in *Inelastic Scattering of Neutrons* (International Atomic Energy Agency, Vienna, 1965), Vol. I, p. 181.

[25] F. Herman and S. Skillman, *Atomic Structure Calculations* (Prentice-Hall, Inc., Englewood Cliffs, N. J., 1963).

[26] J. C. Slater, Phys. Rev. **81**, 385 (1951).

[27] W. Kohn and L. J. Sham, Phys. Rev. **140**, A1133 (1965).

[28] J. E. Robinson, F. Bassani, R. S. Knox, and J. R. Schrieffer, Phys. Rev. Letters **9**, 215 (1962).

[29] T. L. Loucks and R. H. Cutler, Phys. Rev. **133**, A819 (1964).

[30] L. M. Falicov, Phil. Trans. Roy. Soc. London **A255**, 55 (1962).

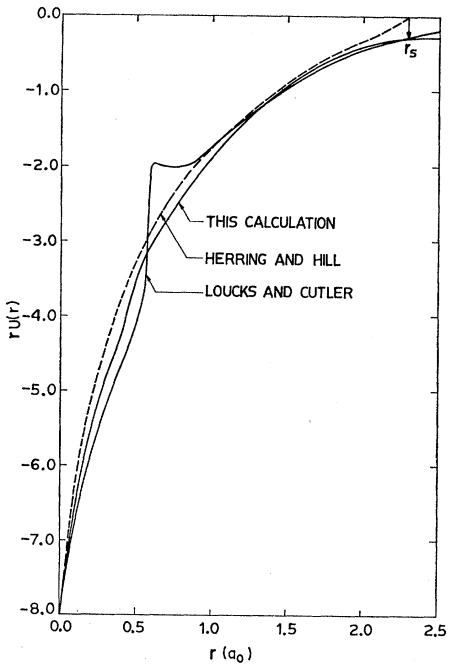

FIG. 2. The crystal potential for Be. The radial distance r is expressed in Bohr units (a_0) and the potential $U(r)$ is measured in Rydbergs.

potential calculated by us in the manner described above, the calculated phonon frequencies come out to be imaginary for low $\mathbf{q}$ values for the longitudinal acoustic branch in the [0001] direction. In the longitudinal branch in the low $\mathbf{q}$ region, the contribution from the normal processes dominates and this contribution is determined by the value of $U_s(p)$ for small p. In other words, the trouble may be due to the inaccuracy of the calculated crystal potential near the cell boundary. Our guess was found to be quite true when a comparison of the potential was made with more accurate potentials of Loucks and Cutler and of Falicov. Instead of trying to construct a very accurate potential, which would have led to lengthy calculations, we circumvented the difficulty by introducing a parameter λ in the screened-exchange potential of conduction electrons, i.e.,

$$U_e(r)=2(3/r_s-r^2/r_s^3)-(1.5392/r_s)\lambda R(\alpha), \quad \text{for } r\leq r_s \quad (27a)$$

$$=4/r-(1.5392/r_s)\lambda R(\alpha), \quad \text{for } r>r_s. \quad (27b)$$

The parameter λ is chosen to achieve agreement between calculated and experimental phonon frequencies. The values of λ are 1.984, 1.190, and 1.072 for Be, Mg, and Zn, respectively. The crystal potentials obtained after this modificaton and subsequently used in this calculation are shown in Figs. 2–4. In Fig. 2, the calculated crystal potential for Be is compared with the potentials due to Loucks and Cutler, and to Herring and Hill.[31] As mentioned before, the hump in the Loucks-Cutler potential at $r=0.6a_0$ is due to the exchange potential between core and the conduction electrons which changes its sign at $r=0.6a_0$. In Fig. 3,

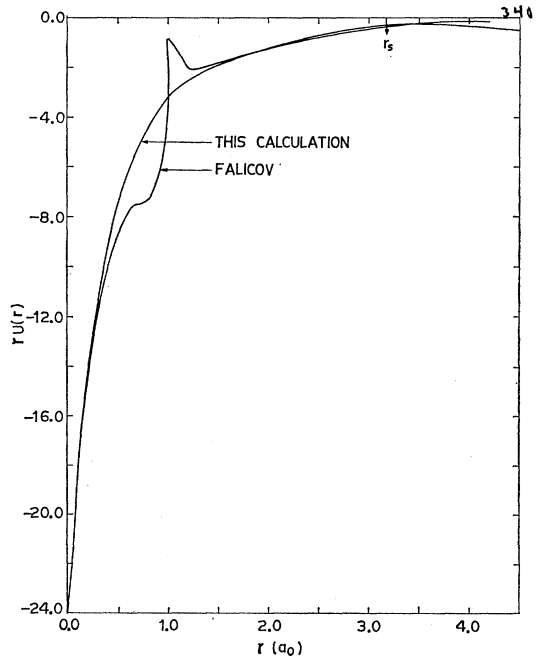

FIG. 3. The crystal potential for Mg. The description of the units is the same as for Fig. 2.

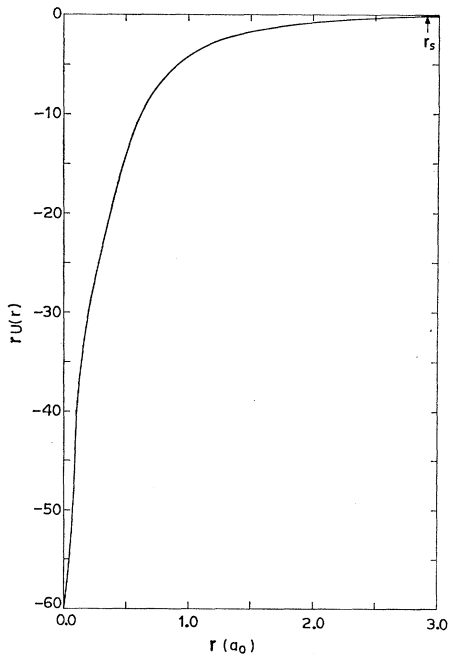

FIG. 4. The crystal potential for Zn. The description of the units is the same as for Fig. 2.

[31] C. Herring and A. G. Hill, Phys. Rev. **58**, 132 (1940).

the calculated crystal potential for Mg agrees well with the potential due to Falicov except for the humps in the region $r=0.4a_0$ to $1.5a_0$. For Zn, no other tabulation of the crystal potential was available to us, so that Fig. 4 shows only the potential calculated by us. The potentials calculated by us agree well with the Loucks-Cutler and Falicov potentials for Be and Mg, respectively, in the vicinity of r_s. The core eigenvalues obtained by the solution of Schrödinger equation for the calculated crystal potential are given in Table I. The addition of a small constant term in the potential hardly affects the core eigenvalues and core eigenfunctions, but the Fourier transform of the potential, which is presented in Fig. 5, changes appreciably for small values of p.

III. RESULTS AND DISCUSSION

We tabulate in Table II the physical parameters used in this calculation for the metals under consideration. The Coulomb coefficients are evaluated with the help of Eqs. (5) and (6) along two principal symmetry directions, [0001] and [01$\bar{1}$0], for a selected set of phonon wave vectors used in this calculation. These coefficients are tabulated in Tables III–V for Be, Mg, and Zn, respectively. The notation for the dynamical matrix is the same as that used by Iyengar *et al.*[2] Roy *et al.*[5] also tabulated these coefficients for Mg, but for ideal ratio $c/a=1.632$, whereas our calculations are for the observed ratios for these metals.

The expansion coefficients A_i, B_i, and C_i are calculated by the procedure discussed in the previous paper.[12] The normalizing constant of the single-OPW function has been ignored in this calculation also. The functions $U_s(p)$ and $U_0(p)$ and the expansion coefficients A_i, B_i, and C_i are tabulated in Tables VI–VIII for Be, Mg, and Zn, respectively. The coefficient A_i decreases in magnitude with increasing p, but not as rapidly as we expect. It is for this reason that $A_i(p)$ does not cancel $U_s(p)$, and $E_{xy}^{(1)}(p)$ defined by Eq. (11) does not converge quickly. Other coefficients A_2, B_i, and C_i are either divergent or oscillatory; consequently, $E_{xy}^{(2)}(p)$ of Eq. (12) does not all off rapidly.

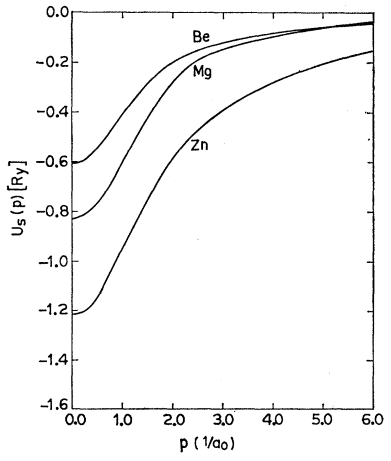

FIG. 5. The Fourier transforms of crystal potentials for Be, Mg, and Zn. The p is in units of $(1/a_0)$ and $U_s(p)$ is in Rydbergs.

TABLE I. Core eigenvalues of Be, Mg, and Zn ($-E$ is in Rydberg units).

State \ Metal	$_4$Be	$_{12}$Mg	$_{30}$Zn
$1s$	5.4440	87.7821	674.2685
$2s$		3.8031	76.0513
$2p$		1.4702	66.7887
$3s$			5.8249
$3p$			3.0767
$3d$			0.9445

We have calculated the functions $G^{(1)}(p)$ and $G^{(2)}(p)$, defined by the relations

$$E_{xy}^{(1)}(p)=-4\pi Z^{*2}e^2(p_xp_y/p^2)G^{(1)}(p) \qquad (28)$$

and

$$E_{xy}^{(2)}(p)=-4\pi Z^{*2}e^2(p_xp_y/p^2)G^{(2)}(p), \qquad (29)$$

for the three hcp metals. The polarization function due to Singwi *et al.* is used. The functions $G^{(1)}(p)$ and $G^{(2)}(p)$ are shown in Fig. 6. The $G^{(1)}(p)$ is presented in an amplified scale for $p>1.5$. For Be, the functions $G^{(1)}(p)$ and $G^{(2)}(p)$ converge very slowly and have the highest values of these three metals. In the case of Mg, the function $G^{(1)}(p)$ converges but the function $G^{(2)}(p)$ diverges. The relative magnitudes of these functions are found to be in reverse order to the relative values of the atomic radii, which is r_s for these metals.

For alkali metals, we had found that the single-OPW EIME is not very reliable for large values of p. There, we had arbitrarily adjusted $G^{(1)}(p)$ and $G^{(2)}(p)$ for large p, such that the functions vanished beyond a certain

TABLE II. The physical parameters for Be, Mg, and Zn.

Parameters	$_4$Be	$_{12}$Mg	$_{30}$Zn
Ionic mass M (atomic units)	9.012	24.312	65.370
Lattice constant a (in units of Bohr radius a_0)	4.3192	6.0462	5.0358
Lattice constant c (in units of a_0)	6.7714	9.8091	9.3480
Ratio c/a	1.5677	1.6223	1.8565
Volume of the unit cell (in units of a_0^3)	109.4027	310.5576	205.3026
Atomic volume (in units of a_0^3)	54.7013	155.2788	102.6513
Radius of Wigner-Seitz sphere (in units of a_0)	2.3545	3.3335	2.9047
Radius of free-electron Fermi sphere (in units of $1/a_0$)	1.0268	0.7251	0.8325
Plasma frequency (10^{12} cps)	49.2171	17.7856	13.3404
Effective charge Z^*	2	2	2
$\zeta=0.5\ \Omega_0/8\pi a_0Z^*$ (in units of a_0^2)	1.08824	3.0892	2.0442

value of p, and at the same time the adjusted functions led to the values of the phonon frequencies in best possible agreement with the experiments. Here, instead of arbitrary adjustment, we have damped the functions $G^{(1)}(p)$ and $G^{(2)}(p)$ by suitable damping factors. The summation over $\mathbf{H}$ in Eqs. (18) and (19) is taken over 500 nearest reciprocal-lattice points. The damped function $G(p)$ should become vanishingly small for the maximum value of p within the range of the summation over $\mathbf{H}$; otherwise the calculated acoustic and

TABLE III. Coulomb coefficients for Be [in units of $(4\pi Z^{*2}e^2/M\Omega_0)$].

[0001] direction

$q/q_{\max}$	$D_{xx}(\mathbf{q},jj)$	$D_{yy}(\mathbf{q},jj)$	$D_{zz}(\mathbf{q},jj)$	$D_{xx}(\mathbf{q},jj')$	$D_{yy}(\mathbf{q},jj')$	$D_{zz}(\mathbf{q},jj')$
0.2	0.05513	0.05513	1.88971	−0.05251	−0.05251	0.10503
0.4	0.05493	0.05493	1.89010	−0.04467	−0.04467	0.08934
0.6	0.05469	0.05469	1.89059	−0.03245	−0.03245	0.06489
0.8	0.05449	0.05449	1.89099	−0.01706	−0.01706	0.03411
1.0	0.05442	0.05442	1.89114	0.0	0.0	0.0

[01$\bar{1}$0] direction

				$D_{xx}(\mathbf{q},jj')$		$D_{yy}(\mathbf{q},jj')$		$D_{zz}(\mathbf{q},jj')$	
$q/q_{\max}$	$D_{xx}(\mathbf{q},jj)$	$D_{yy}(\mathbf{q},jj)$	$D_{zz}(\mathbf{q},jj)$	Re	Im	Re	Im	Re	Im
0.2	0.06976	1.08654	0.84367	−0.05691	0.03302	0.89016	−0.03438	−0.83324	0.00136
0.4	0.10805	1.16310	0.72882	−0.06128	0.06396	0.74608	−0.07494	−0.68480	0.01096
0.6	0.15571	1.24764	0.59662	−0.06631	0.09021	0.55565	−0.12756	−0.48934	0.03734
0.8	0.19455	1.30862	0.49680	−0.06927	0.10871	0.35654	−0.19775	−0.28728	0.08904
1.0	0.20945	1.33029	0.46024	−0.06754	0.11698	0.16761	−0.29033	−0.10008	0.17335

TABLE IV. Coulomb coefficients for Mg [in units of $(4\pi Z^{*2}e^2/M\Omega_0)$].

[0001] direction

$q/q_{\max}$	$D_{xx}(\mathbf{q},jj)$	$D_{yy}(\mathbf{q},jj)$	$D_{zz}(\mathbf{q},jj)$	$D_{xx}(\mathbf{q},jj')$	$D_{yy}(\mathbf{q},jj')$	$D_{zz}(\mathbf{q},jj')$
0.2	0.04704	0.04704	1.90593	−0.04478	−0.04478	0.08957
0.4	0.04690	0.04690	1.90620	−0.03809	−0.03809	0.07619
0.6	0.04674	0.04674	1.90654	−0.02768	−0.02768	0.05535
0.8	0.04660	0.04660	1.90681	−0.01455	−0.01455	−0.02910
1.0	0.04654	0.04654	1.90691	0.0	0.0	0.0

[01$\bar{1}$0] direction

				$D_{xx}(\mathbf{q},jj')$		$D_{yy}(\mathbf{q},jj')$		$D_{zz}(\mathbf{q},jj')$	
$q/q_{\max}$	$D_{xx}(\mathbf{q},jj)$	$D_{yy}(\mathbf{q},jj)$	$D_{zz}(\mathbf{q},jj)$	Re	Im	Re	Im	Re	Im
0.2	0.06214	1.08320	0.85470	−0.04866	0.02886	0.89482	−0.03015	−0.84616	0.00129
0.4	0.10172	1.17088	0.72744	−0.05271	0.05595	0.74317	−0.06643	−0.69046	0.01048
0.6	0.15100	1.26692	0.58213	−0.05744	0.07899	0.54629	−0.11483	−0.48884	0.03584
0.8	0.19116	1.33566	0.47325	−0.06037	0.09524	0.34468	−0.18132	−0.28431	0.08608
1.0	0.20656	1.35997	0.43353	−0.05913	0.10242	0.15678	−0.27156	−0.09765	0.16914

TABLE V. Coulomb coefficients for Zn [in units of $(4\pi Z^{*2}e^2/M\Omega_0)$].

[0001] direction

$q/q_{\max}$	$D_{xx}(\mathbf{q},jj)$	$D_{yy}(\mathbf{q},jj)$	$D_{zz}(\mathbf{q},jj)$	$D_{xx}(\mathbf{q},jj')$	$D_{yy}(\mathbf{q},jj')$	$D_{zz}(\mathbf{q},jj')$
0.2	0.02347	0.02347	1.95305	−0.02234	−0.02234	0.04467
0.4	0.02345	0.02345	1.95310	−0.01900	−0.01900	0.03800
0.6	0.02342	0.02342	1.95318	−0.01381	−0.01381	0.02761
0.8	0.02338	0.02338	1.95324	−0.00726	−0.00726	0.01451
1.0	0.02337	0.02337	1.95326	0.0	0.0	0.0

[01$\bar{1}$0] direction

				$D_{xx}(\mathbf{q},jj')$		$D_{yy}(\mathbf{q},jj')$		$D_{zz}(\mathbf{q},jj')$	
$q/q_{\max}$	$D_{xx}(\mathbf{q},jj)$	$D_{yy}(\mathbf{q},jj)$	$D_{zz}(\mathbf{q},jj)$	Re	Im	Re	Im	Re	Im
0.2	0.04067	1.08230	0.87703	−0.02456	0.01595	0.90273	−0.01693	−0.87818	0.00098
0.4	0.08587	1.22158	0.69257	−0.02735	0.03108	0.71897	−0.03917	−0.69162	0.00809
0.6	0.14213	1.36821	0.48967	−0.03074	0.04412	0.49883	−0.07254	−0.46810	0.02843
0.8	0.18797	1.46940	0.34265	−0.03314	0.05335	0.29349	−0.12408	−0.26036	0.07072
1.0	0.20556	1.50444	0.29003	−0.03306	0.05727	0.11684	−0.20238	−0.08378	0.14512

TABLE VI. $U_s(p)$, $U_0(p)$, and expansion coefficients for Be [p is in units of $(1/a_0)$; $U_s(p)$, $U_0(p)$, and A_1, B_1, and C_1 are in Rydbergs; A_2, B_2, and C_2 are dimensionless].

p	$U_s(p)$	$U_0(p)$	A_1	B_1	C_1	A_2	B_2	C_2
0.2	−0.82039	−0.19891	0.62148	−0.00789	0.00010	0.07282	−0.00169	0.00003
0.5	−0.76914	−0.16787	0.60127	−0.04540	0.00347	0.06850	−0.00952	0.00089
0.7	−0.71487	−0.13468	0.58019	−0.08129	0.01161	0.06411	−0.01664	0.00289
1.0	−0.61332	−0.07213	0.54119	−0.13898	0.03690	0.05628	−0.02716	0.00880
1.25	−0.52033	−0.01500	0.50533	−0.18225	0.06880	0.04942	−0.03404	0.01577
1.50	−0.42921	0.03979	0.46900	−0.21680	0.10613	0.04280	−0.03849	0.02336
2.0	−0.27863	0.12205	0.40068	−0.25801	0.17875	0.03135	−0.04033	0.03620
2.5	−0.18690	0.15506	0.34196	−0.27091	0.23289	0.02266	−0.03759	0.04291
3.0	−0.14166	0.15163	0.29329	−0.26715	0.26765	0.01639	−0.03212	0.04398
3.5	−0.11618	0.13729	0.25347	−0.25410	0.28552	0.01196	−0.02636	0.04130
4.0	−0.09333	0.12767	0.22100	−0.23721	0.28442	0.00885	−0.02123	0.03656
4.5	−0.07191	0.12238	0.19429	−0.22116	0.27004	0.00664	−0.01703	0.03131
5.0	−0.05721	0.11469	0.17190	−0.20781	0.25479	0.00505	−0.01373	0.02655
5.5	−0.05023	0.10254	0.15277	−0.19697	0.23871	0.00389	−0.0114	0.02240
6.0	−0.04620	0.08991	0.13611	−0.18832	0.22994	0.00302	−0.00911	0.01903

TABLE VII. $U_s(p)$, $U_0(p)$, and the expansion coefficients for Mg (the units are the same as in Table VI).

p	$U_s(p)$	$U_0(p)$	A_1	B_1	C_1	A_2	B_2	C_2
0.2	−0.59824	−0.06926	0.52898	0.00596	−0.00036	−0.05358	0.00682	−0.00024
0.5	−0.54831	−0.04128	0.50703	0.03087	−0.01033	−0.04255	0.03489	−0.00729
0.7	−0.49802	−0.01509	0.48293	0.05192	−0.02878	−0.03302	0.05538	−0.02169
1.0	−0.41133	0.02592	0.43725	0.08928	−0.06975	−0.01980	0.07584	−0.05563
1.25	−0.34074	0.05490	0.39564	0.12986	−0.11170	−0.01167	0.08136	−0.08524
1.50	−0.28000	0.07470	0.35470	0.18013	−0.16258	−0.00636	0.07956	−0.10799
2.0	−0.19726	0.08401	0.28127	0.29924	−0.30014	0.00161	0.06814	−0.13046
2.5	−0.15193	0.06944	0.22137	0.42537	−0.47627	−0.00057	0.05641	−0.13470
3.0	−0.12126	0.05255	0.17381	0.54402	−0.66663	−0.00064	0.04652	−0.12742
3.5	−0.09823	0.03740	0.13563	0.64843	−0.86442	−0.00093	0.03888	−0.11614
4.0	−0.08245	0.02205	0.10450	0.73777	−1.07637	−0.00117	0.03281	−0.10649
4.5	−0.07015	0.00869	0.07884	0.80862	−1.31019	−0.00129	0.02764	−0.09610
5.0	−0.05892	−0.00109	0.05783	0.86035	−1.62986	−0.00130	0.02318	−0.09157
5.5	−0.05023	−0.00880	0.04143	0.89369	−1.70586	−0.00122	0.01876	−0.07834
6.0	−0.04431	−0.01565	0.02866	0.92241	−1.68796	−0.00113	0.01526	−0.06133

optical frequencies in the [0001] direction will not remain degenerate at the zone boundary as demanded by symmetry. Our choice of the damping factor was governed by this requirement. The dynamical matrices $D_{xy}(\mathbf{q},jj')$ and $D_{xy}(\mathbf{q},jj)$ are obtained by adding the Coulombic and electronic contributions, and the phonon frequencies are calculated with the help of Eqs. (20) and (21).

We shall now discuss the results for each metal separately.

A. Beryllium

$U_0(p)$ changes its sign at $p=1.25$. Here, and henceforth, p is measured in units of $(1/a_0)$. We use the damping factors $\exp[-0.03(p/2k_F)^4]$ and

$$\{\exp[-0.03(p/0.5k_F)^4]\}^2,$$

which multiply $G^{(1)}(p)$ and $G^{(2)}(p)$, respectively. The damped function $G(p)=[G^{(1)}(p)+G^{(2)}(p)]$ shown in Fig. 7 does become vanishingly small within the sphere of summation of **H**. In Fig. 7, we also show the function $G(p)$ due to Animalu[32] which becomes negligible for $p>3.0$.

[32] A. E. O. Animalu, Proc. Roy. Soc. (London) **A294**, 376 (1935).

In Fig. 8, the calculated phonon frequencies for Be for the two principal symmetry directions [0001] and [01$\bar{1}$0] are compared with the phonon dispersion curves measured by Schmunk.[1] The agreement between the calculated and experimental phonon frequencies is good except for the transverse optical (TO) and the longitudinal optical (LO) branches in the [01$\bar{1}$0] direction for intermediate and large values of phonon

TABLE VIII. $U_s(p)$, $U_0(p)$, and the expansion coefficients for Zn (the units are the same as in Table VII).

p	$U_s(p)$	$U_0(p)$	A_1	B_1	C_1
0.2	−1.20298	−0.09609	1.10689	0.00265	0.00030
0.5	−1.14036	−0.06869	1.07167	0.01809	0.00961
0.7	−1.07516	−0.04020	1.03496	0.03533	0.03174
1.0	−0.95630	0.00842	0.96472	0.06502	0.11335
1.25	−0.85097	0.04512	0.89609	0.09312	0.25133
1.50	−0.75067	0.07200	0.82267	0.12868	0.46600
2.0	−0.58702	0.08903	0.67605	0.22442	1.13752
2.5	−0.47447	0.06874	0.54321	0.33435	2.14524
3.0	−0.39262	0.03668	0.42930	0.43011	3.48924
3.5	−0.32663	0.00738	0.33401	0.49424	5.14866
4.0	−0.27448	−0.01828	0.25560	0.52108	7.05108
4.5	−0.23487	−0.04376	0.19111	0.50889	9.21676
5.0	−0.20246	−0.06422	0.13824	0.45867	11.58772
5.5	−0.17374	−0.07833	0.09541	0.37394	14.03231
6.0	−0.14965	−0.08872	0.06093	0.26231	16.56654

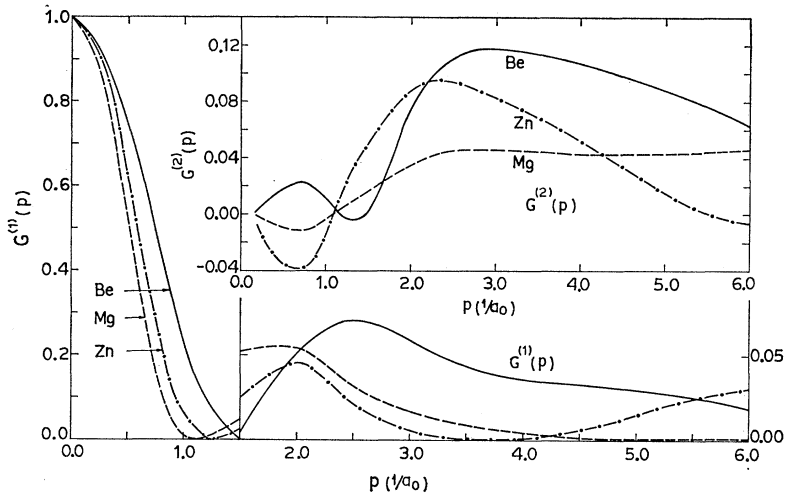

FIG. 6. The undamped functions $G^{(1)}(p)$ and $G^{(2)}(p)$ for Be, Mg, and Zn. The $G^{(1)}(p)$ for $p>1.5$ is presented in an amplified scale. The $G^{(2)}(p)$ is shown in the upper right-hand corner.

wave vector. An enigmatic feature of the calculation is that, in the [01$\bar{1}$0] direction, the calculated LO branch lies above the TO(||), while the experimental measurements show that the situation is just the reverse. The phonon frequencies for the TO($\perp$) mode in the [01$\bar{1}$0] direction show a little dispersion over the range of $\mathbf{q}$ values.

Koppel and Yong[10] employed the pseudopotential method developed by Sham[33] to calculate the phonon frequencies of Be. They used the polarization function of Hubbard,[23] the bare-ion potential of Loucks and Cutler,[29] and neglected the core-core exchange repulsion. Their results in the [0001] direction are in good agreement with experiment except for the TO branch, while the agreement is poor in the [01$\bar{1}$0] direction. They extended their calculations using a dielectric function based on 23 OPW's, but this improvement led to disappointing results. Brovman, Kagan, and Holas[8] used the Heine-Animalu potential to calculate the phonon frequencies of Be. They obtained good agreement with experiment by adjusting three parameters which enter their calculations.

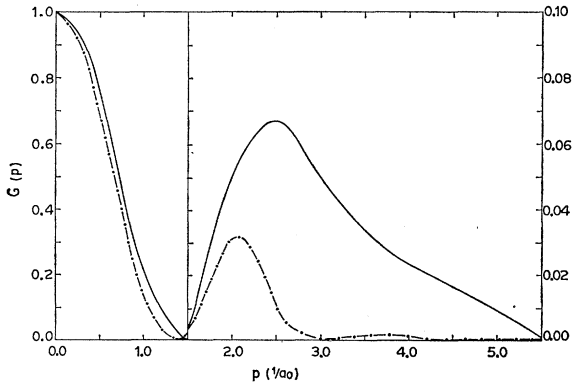

FIG. 7. The damped function $G(p)$ for Be. The function $G(p)$ for $p>1.5$ is shown in an amplified scale. Solid curve represents the present calculation, whereas the dot-dash curve is from Animalu.

[33] L. J. Sham, Proc. Roy. Soc. (London) A283, 33 (1965).

B. Magnesium

$U_0(p)$ shows oscillatory behavior for Mg. It is positive from $p=0.8$ to 4.8. The function $U_0(p)$ interferes with the function $\mathcal{G}(pr_s)$ constructively for p values where the two functions have the opposite signs and destructively for p values where they have the same sign. $G^{(1)}(p)$ becomes almost zero for $p>5.25$, and there is no necessity of damping this function. $G^{(2)}(p)$ diverges and is, therefore, damped by the factor

$$-\exp[-0.03(p/2k_F)^4].$$

The $G(p)$ function obtained in this manner is plotted in

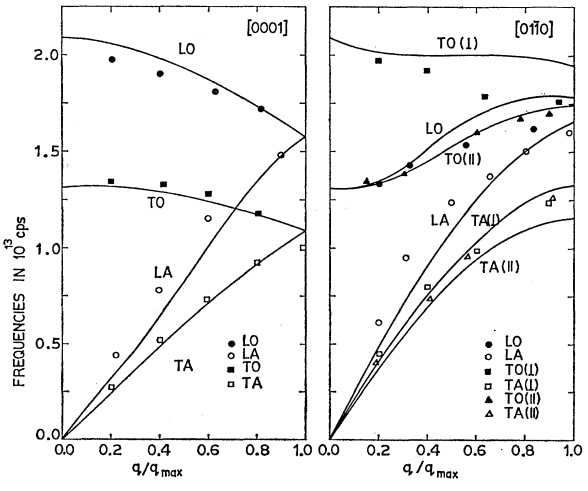

FIG. 8. The phonon dispersion curve for Be in the [0001] and the [01$\bar{1}$0] directions. The experimental points are from Schmunk (Ref. 1), while the solid curves represent the present calculation. In the [01$\bar{1}$0] direction, || and $\perp$ denote that the polarization vectors are parallel and perpendicular to the basal plane for the corresponding transverse branches.

Fig. 9. For comparison, the corresponding curve obtained by Animalu is also given.

The calculated phonon frequencies in the two principal symmetry directions, [0001] and [01$\bar{1}$0], are compared in Fig. 10 with the neutron spectrometric measurements of Iyengar *et al.*[2] We have also plotted the frequencies calculated by Roy *et al.*, who used the two-parameter-model pseudopotential of Harrison. Roy *et al.* assumed the ideal ratio ($c/a=1.632$) for Mg, whereas we have used the observed value $c/a=1.6223$. Because of the use of a different c/a value, we found that the frequencies for the observed c/a increase at the most by 3% in the longitudinal branches when compared with frequencies corresponding to ideal c/a ratio, except in the longitudinal acoustic branch in the [0001] direction for the low $\mathbf{q}$ region, where the frequencies decrease up to 8%. There is no appreciable change in the frequencies of transverse phonons. Schneider and Stoll[9] generated a four-parameter-model pseudopotential by forcing a fit with the observed phonon frequencies and used the pseudopotential thus obtained to explain the electronic band structure, the cohesive energy, the Fermi surface, the crystal stability, the interatomic potential, and the electrical resistivity of Mg.

We note that in the [0001] direction the frequencies for the LO and the LA branches are in good agreement with the experimental data. The worst deviation from experiment, which occurs for the TO and the TA branches, is 25%. A noticeable discrepancy with experiment in the [01$\bar{1}$0] direction is that the TA($\|$) branch lies above the TA($\perp$) branch. A comparable agreement was achieved in the calculations of Roy *et al.*, but the dispersion curves calculated by us and by Roy *et al.* lie mostly on opposite sides of the experimental values.

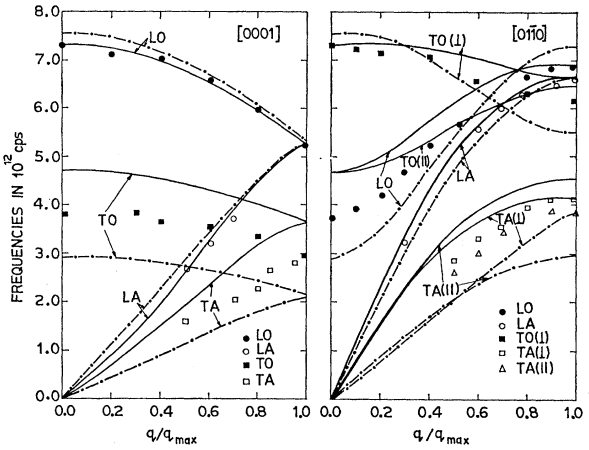

FIG. 10. The phonon dispersion curves for Mg in the [0001] and [01$\bar{1}$0] directions. The experimental points are from Iyengar *et al.* (Ref. 2). The solid curves correspond to this calculation while dot-dash curves are from Roy *et al.* (Ref. 5). The explanation for $\|$ and $\perp$ is the same as for Fig. 8.

C. Zinc

The numerical integrations involved in the evaluation of expansion coefficients A_i, B_i, and C_i increase greatly in complexity with increasing atomic number. With the intention of avoiding complicated and lengthy calculations, we ignored the coefficients A_2, B_2, and C_2 in our calculations for Zn. This approximation should not affect the final phonon frequencies, because the function $G^{(2)}(p)$ is heavily damped and the errors in the evaluation of undamped $G^{(2)}$ will be suppressed. The general behavior of $U^0(p)$ is the same as in the case of Mg. In order to ensure that the functions $G^{(1)}(p)$ and $G^{(2)}(p)$ are reduced to negligible values within the range of summation over $\mathbf{H}$, we multiply these functions by the damping factors $\{\exp[-0.03(p/2k_F)^4]\}^2$ and $\{0.5\exp[-0.03(p/0.5k_F)^4]\}^2$, respectively. The function $G(p)$ finally obtained by us and the same function from Animalu are displayed in Fig. 11.

In Fig. 12, we compare the phonon frequencies calculated by us in the [0001] and [01$\bar{1}$0] directions with the measurements of McDonald *et al.*[3] The agreement achieved is good in the [0001] direction, while in the

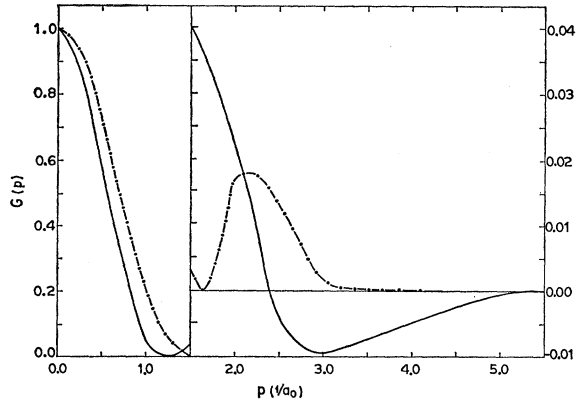

FIG. 9. The damped function $G(p)$ for Mg. The description of the figure is the same as for Fig. 7.

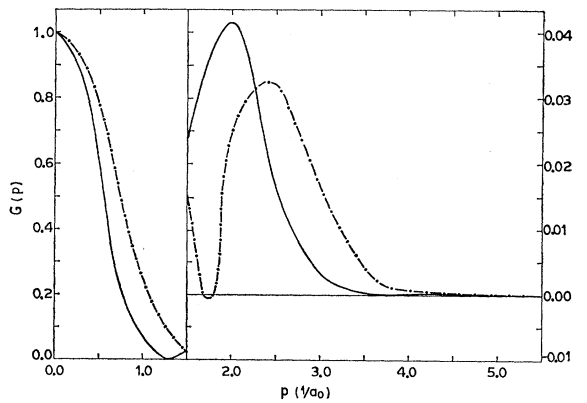

FIG. 11. The damped function $G(p)$ for Zn. The description of the figure is the same as for Fig. 7.

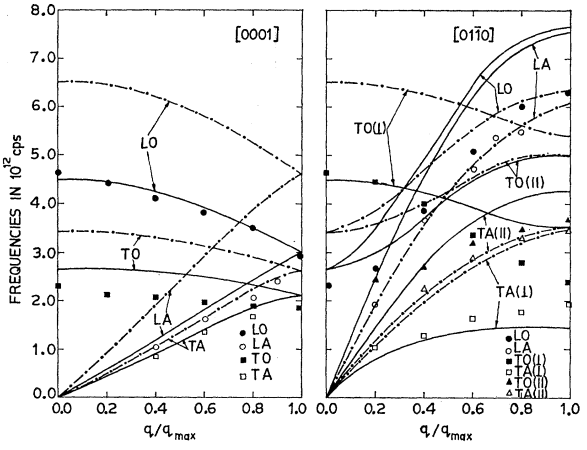

FIG. 12. The phonon dispersion curves for Zn in the [0001] and [01$\bar{1}$0] directions. The experimental points are from McDonald *et al.* The solid curves are for the observed ratio $c/a=1.8565$, while the dot-dash curves are for the ideal ratio $c/a=1.6333$.

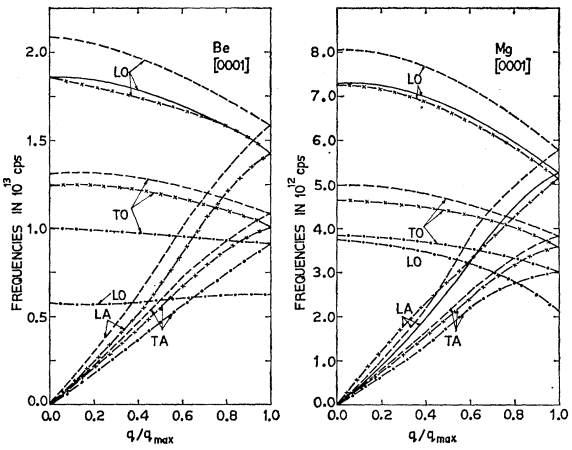

FIG. 13. The phonon dispersion curves for Be and Mg in the [0001] direction for different values of the ratio c/a: dash line for $c/a=1.5677$; solid line for $c/a=1.6223$; dash-x-dash line for $c/a=1.6333$; dash-dot-dash line for $c/a=1.8565$. TA and TO branches for $c/a=1.6223$ and 1.6333 almost overlap.

[01$\bar{1}$0] direction the agreement is poor for all branches except the TA(⊥) branch. The measurements of McDonald *et al.* seem to be more detailed and reliable than the measurements of Iyengar *et al.*,[34] which we have not shown in the figure. McDonald *et al.* failed to fit their measurements with two-parameter pseudopotential calculations.

D. Homologous Correspondence in Be, Mg, and Zn

The two transverse acoustic branches in the [01$\bar{1}$0] direction in Be and Mg lie close together. For these two metals, the velocities of the two transverse sound waves are nearly equal. But for Zn, the above two branches lie strikingly far apart. Similar differences exist between Zn and the other two metals for the TO(∥) and the LO branches in the [01$\bar{1}$0] direction. Thus, among these hcp metals, Be and Mg show a homologous behavior, whereas Zn seems to stand apart.

The distinctive features of Zn and its anisotropy are related to its large (1.8565) c/a ratio. We thought that it would be interesting to study the variation of the phonon frequencies with the variation of c/a ratio keeping the volume of the unit cell constant. The dot-dash lines in Fig. 12 show the phonon frequencies for Zn for $c/a=1.6333$ (ideal ratio). The agreement with experiment in the [0001] direction that we had earlier for the real c/a ratio is completely lost. In the [01$\bar{1}$0] direction, good agreement is obtained for TA(∥) and LA branches. It is interesting that the TA(⊥) and the TA(∥) branches now show the features homologous to those for Be and Mg.

We also calculated the phonon frequencies in the [0001] direction for Be and Mg for different values of c/a keeping the volume of the unit cell constant. In Fig. 13, we compare the phonon frequencies calculated for four values of c/a which are equal to 1.5677 (observed for Be), 1.6223 (observed for Mg), 1.6333 (ideal), and 1.8565 (observed for Zn). We observe that except for the LA branch for Mg for $q<0.6q_{max}$, the phonon frequencies decrease with increasing c/a because the Coulombic contribution decreases faster than the electronic contribution with an increase in c/a. It is important to note that for $c/a=1.8565$ phonon frequencies become imaginary for the LA branch for both Mg and Be, the frequencies for LO branch assume extremely low values, and the LO branch lies below the TO branch. Be and Mg are, therefore, unstable as hcp structures for a c/a value equal to that observed for Zn.

[34] P. K. Iyengar, G. Venkataraman, Y. H. Gameel, and K. R. Rao, in *Inelastic Scattering of Neutrons* (International Atomic Energy Agency, Vienna, 1968), Vol. I, p. 124.

ACKNOWLEDGMENTS

We are grateful to the Council of Scientific and Industrial Research, India, for financial support. We are also thankful to the authorities of the Tata Institute of Fundamental Research, Bombay, for allowing us to use their computer center facilities. It is a pleasure to acknowledge several informative discussions with Dr. G. Venkataraman.